The IFMIF High Energy Beam Transport line

-

Error studies

R. Duperrier, J. Payet, D. Uriot

CEA Saclay 91191 Gif sur Yvette

Abstract

The IFMIF project (International Fusion Materials Irradiation Facility) includes two linacs operating in CW mode to accelerate 125 mA deuteron beams up to 40 MeV. After extraction and transport, the deuteron beams with strong internal space charge forces have to be bunched, accelerated and transported to the liquid lithium target for the production of high neutrons flux. This paper presents the design of the high energy beam transport (HEBT) which provides a flat rectangular beam profile on the target and the beam dynamics end-to-end calculations including errors.

1 REQUIREMENTS

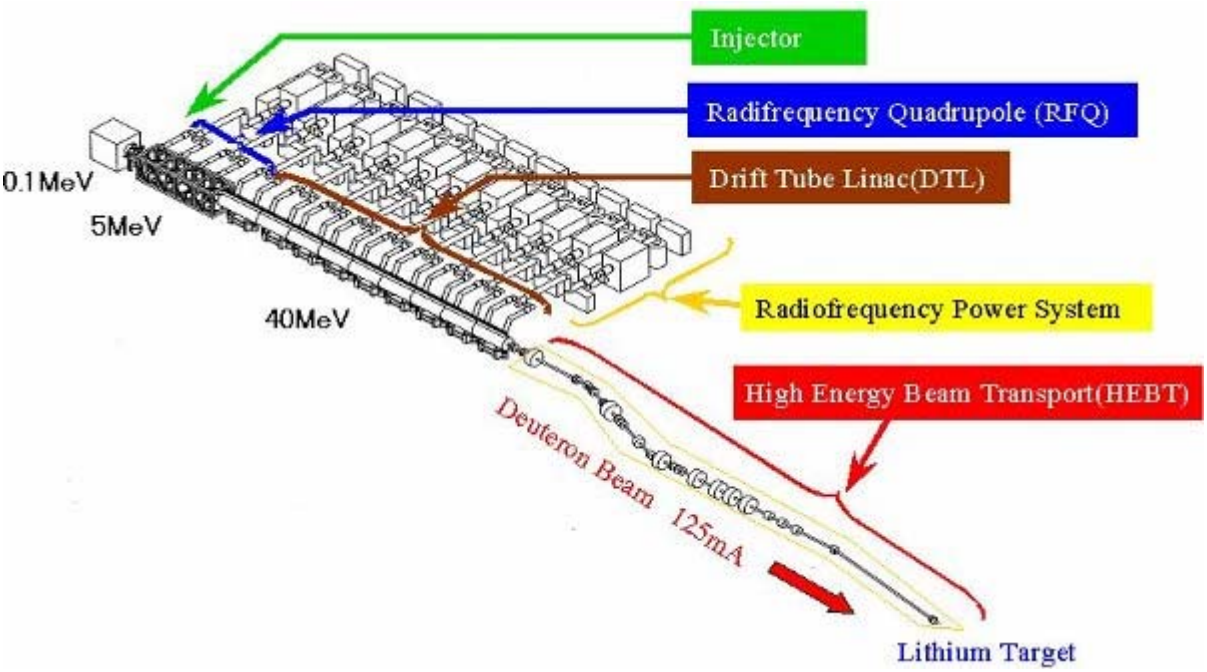

Figure 1: General ifmif accelerator module layout.

The HEBT line has to transport the beam from the exit of the accelerator to the target or the dump with the desired footprint sizes and characteristics. In normal operation, the footprint of each beam must be rectangular, 20 cm horizontal × 5 cm vertical at the flat top. The beam flux has to be approximately uniform (~5 %) across the flat top of the beam profile. The angle at which the beam intercepts the target results from a compromise between maximizing the flux in the test cell and minimizing the activation due to back streaming neutrons. These two considerations indicate an optimum around 10°.
The horizontal separation between the target center and the axis of the linac, needed for concrete shielding, was estimated around 6.40 m by considering the A.E.S (Advanced Energy System, Inc.) design [2].

2 GENERAL DESCRIPTION OF THE HEBT

The incidence angle of each beam at the target is obtained with one achromat composed with two 4.5° bend. This allows a cost reduction compared to the previous design and an operation simplification. The achromat is located near the accelerating system output. At this location, the energy spread growth induced by the space charge is minimized. The line length after the deviation is set in order to reach the horizontal separation between the target center and the linac reference line. In the present design the separation distance is 5.3 m, as shown in Figure 2, and this can be insufficient, but the lengthening of the last drift can increase this distance. The total line length is 43.12 m. Transverse uniform shape is obtained using non-linear multipole lenses (octupoles and duodecapoles).

The HEBT line is divided in three functional sections:

- The goal of the first section, which includes the achromat, is to match the linac output beam

through the achromat and for the entry in the second section.

- In the second section, the optical conditions (see section 3) are designed in order to allow for insertion of the octupole and duodecapole lenses at 4 positions.
- The last section, including the beam expansion drift, allows the matching of the needed beam sizes at the target.

This organization allows an easy tuning of the line. All the first order simulations are performed with the code BETA [3].

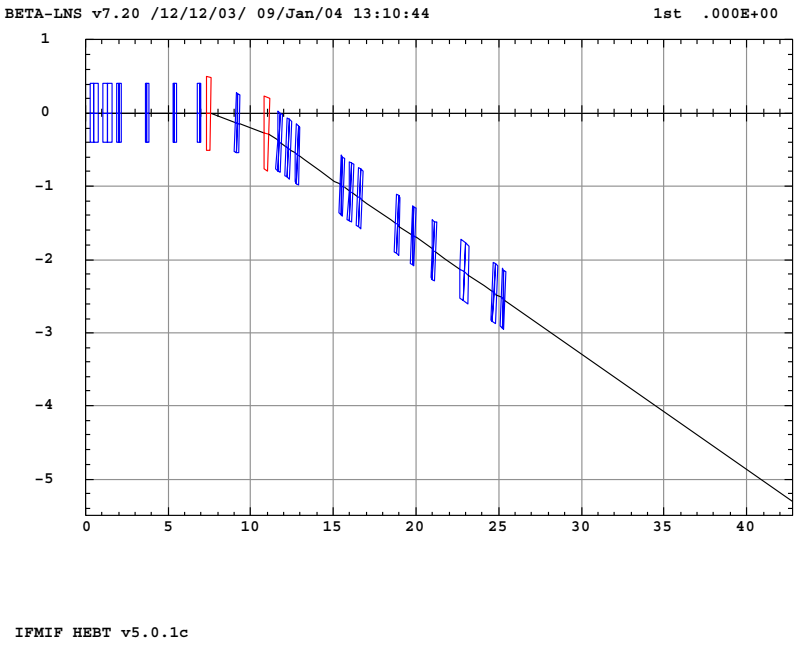

Figure 2: The HEBT Layout.

OCTUPOLE TUNING

The tuning of the octupoles [4][5] assume the following hypothesis:
The transverse motions are supposed to be uncoupled (the space charge coupling is assumed negligible). The non-linear lenses dedicated to the horizontal distribution flatness (and respectively the vertical distribution) are supposed to be located at a waist of the vertical motion (respectively the horizontal). This allows to act on one plane with minimized effects on the other plane.
At the horizontal non-linear lenses (and respectively the vertical), the beam ellipses in the horizontal phase spaces (x, x') (respectively the vertical (z, z')) is supposed to be thin enough ($\beta\,\gamma >> 1$).
The beam at the octupolar lenses is described by its rms ellipse frontier:

$$\varepsilon_0 = \gamma_0 y_0^2 + 2\alpha_0 y_0 y_0' + \beta_0 y_0'^2 \quad with\ y = x, z$$

$\beta_0, \alpha_0, \gamma_0 = \dfrac{\left(1+\alpha_0^2\right)}{\beta_0}$ are the optical functions at the lenses and ε_0 is the rms emittance.

As the beam ellipse is assumed thin enough the relationship between y_0 and y_0' is close to the linear regression [4]:

$$y_0 \approx -sign(\alpha_0)\sqrt{\frac{\beta_0}{\gamma_0}}\,y_0' \approx -\frac{\beta_0}{\alpha_0}\,y_0'$$

We consider the octupole case, the phase space coordinates at the target are:

$$\begin{pmatrix} y \\ y' \end{pmatrix} = \begin{pmatrix} T_{11} y_0 + T_{12}\left(y'_0 + OL\, y_0^3\right) \\ T_{21} y_0 + T_{22}\left(y'_0 + OL\, y_0^3\right) \end{pmatrix}$$ where OL is the octupole integrated strength $\left(OL = \frac{\mathbf{B}\, L}{a^3 B\rho}\right)$

with **B** the field at the pole-tip, a the radius at the pole-tip, L the octupole length and T_{11}, T_{12}, T_{21}, T_{22} are the terms of the 1st order transfer matrix between the octupolar lenses and the target.

If the phase space ellipse is flat enough, one may consider that $y_0 \approx -\frac{\beta_0}{\alpha_0} y'_0$, and by replacement in the previous equation this gives:

$$\begin{pmatrix} y \\ y' \end{pmatrix} = \begin{pmatrix} y'_0\left(\frac{-\beta_0}{\alpha_0} T_{11} + T_{12}\right) - OL\, T_{12}\left(\frac{\beta_0 y'_0}{\alpha_0}\right)^3 \\ y'_0\left(\frac{-\beta_0}{\alpha_0} T_{21} + T_{22}\right) - OL\, T_{22}\left(\frac{\beta_0 y'_0}{\alpha_0}\right)^3 \end{pmatrix}$$

The extent of the region of uniform density is comprising between $\pm y_M$, where y_M is defined by:

$$y_M = y'_0(y_M)\left(\frac{-\beta_0}{\alpha_0} T_{11} + T_{12}\right) - OL\, T_{12}\left(\frac{\beta_0 y'_0(y_M)}{\alpha_0}\right)^3 \text{ and } \frac{dy}{dy'_0}\left(y'_0(y_M)\right) = 0$$

By solving the previous equations, one finds:

$$y'_0(y_M) = \pm \frac{\sqrt{\frac{-\beta_0}{\alpha_0} T_{11} + T_{12}}}{\sqrt{3\, OL\, T_{12}\left(\frac{\beta_0}{\alpha_0}\right)^3}}$$

The particular value $y'_0(y_M)$ where the distortion occurs depends on the incoming probability density function f(y'$_0$). When f(y'$_0$) is gaussian with an rms value $\sigma_{y'_0} = \sqrt{\varepsilon_0 \gamma_0}$, it appears [2][3] that an optimum value is $y'_0(y_M) \approx \frac{4}{3}\sigma_{y'_0}$, this gives values for the octupole strength:

$$OL = \frac{3\left(\frac{-\beta_0}{\alpha_0} T_{11} + T_{12}\right)}{16\left(\varepsilon_0 \gamma_0 T_{12}\left(\frac{\beta_0}{\alpha_0}\right)^3\right)},$$

and the uniform density beam extension:

$$y_M = \pm \frac{8}{9}\sqrt{\varepsilon_0 \gamma_0}\left(\frac{-\beta_0}{\alpha_0} T_{11} + T_{12}\right)$$

The two previous expressions depend on the optics between the octupole position and the target $\left(T_{11} = \sqrt{\frac{\beta_t}{\beta_0}}\left(Cos(\Delta\varphi) + \alpha_0 Sin(\Delta\varphi)\right),\ T_{12} = \sqrt{\beta_t \beta_0}\, Sin(\Delta\varphi)\right)$ (where β_t is the betatron function at the target and $\Delta\varphi$ the phase advance between the target and the octupole). All changes in the optics imply the change of the needed octupole strength. In the case of high intensity beam (i.e high space charge strength) the optics is modified. These expressions give the approximate octupole strength.

FIRST ORDER MATCHING DESCRIPTION

- **1st section, Linac to "Multipolar section" matching section:**

Before being able to apply mutipolar lenses forces, one needs a section to match the beam to specific conditions. The quadrupole between the two bending magnets gives the achromatic conditions. The matching of the 6 following conditions is achieved with 6 quadrupoles:

- 2 symmetrical conditions (α_x=0, α_z=0) at the middle of the achromat,
- Matching optical conditions (α_x, β_x, α_z, β_z) at the entry of the 2nd section.

The beam sizes, defined as $\sqrt{\beta_x \varepsilon_x + (D_x \delta)^2}$ in horizontal and $\sqrt{\beta_z \varepsilon_z}$ in vertical, are less than 1.5 cm, with ε_x=6.18 10^{-6} m.rad, ε_z=6.20 10^{-6} m.rad and δ=0 (see Figure 3 and Figure 4).

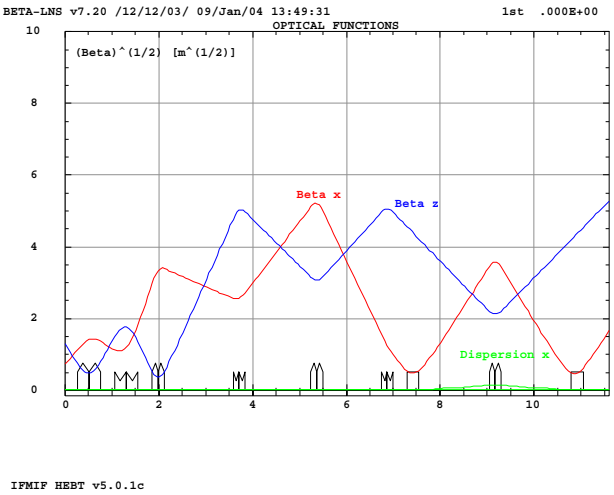

Figure 3: optical functions in the 1st section.

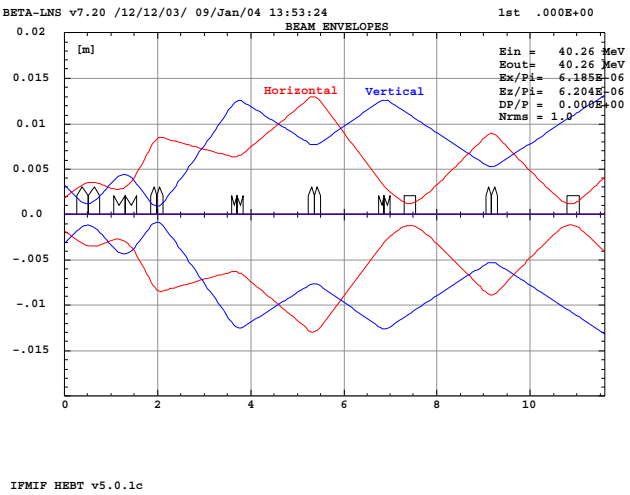

Figure 4: beam envelopes in the 1st section.

- **2nd section, "Multipolar section":**

Multipolar lenses (octupoles, duodecapoles) are used in order to obtain uniform beam density at the target. When the beam sizes, at the multipole location, are small in one plane and large in the other one, the multipole have an effect in the plane where the beam is sufficiently big. Four positions, where the beam sizes have the previous properties, are achieved with 6 quadrupoles. This allows the insertion of 4 multipoles, 2 for each plane. In this section, like the previous section, the beam sizes are less than or equal to 1.5 cm (see Figure 5 and Figure 6).

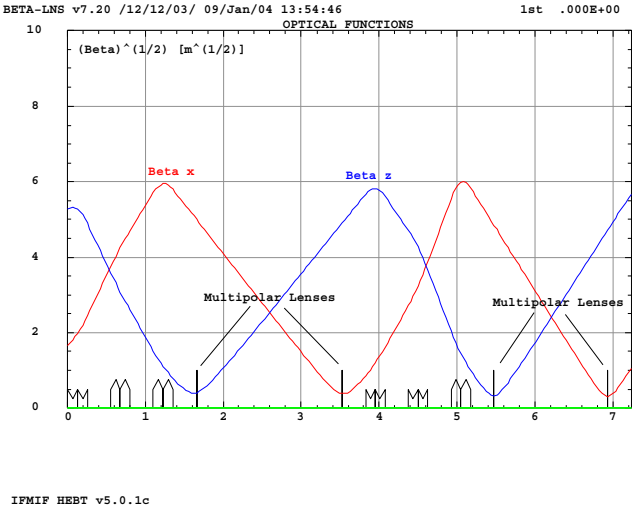

Figure 5: optical functions in the 2nd section.

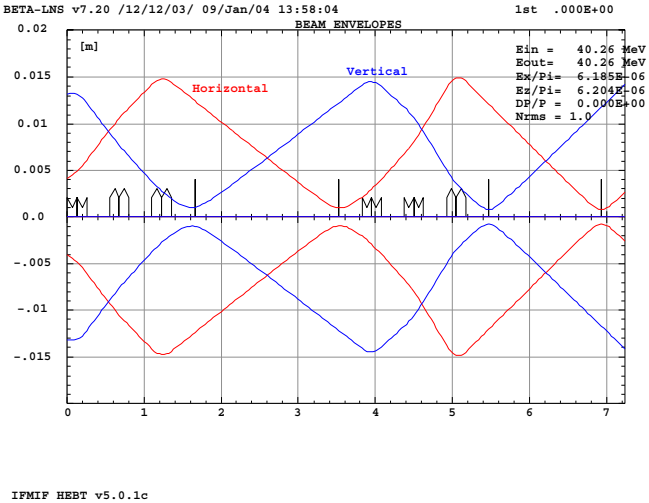

Figure 6: beam envelopes in the 2nd section.

- **3rd section, Footprint matching section:**

The last section has to match the target footprint beam sizes to the requirements. This is made with 6 quadrupoles. Below are showed the full HEBT line optical functions for a 10×5 cm footprint beam size at the target. Figure 7 and Figure 8 show optical functions and beam envelopes of this section.

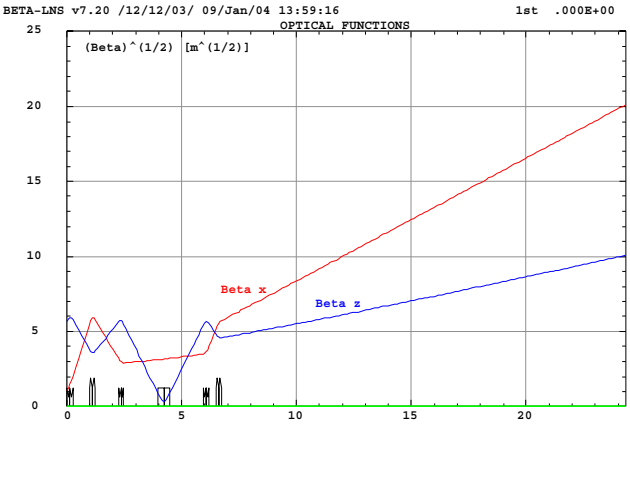

Figure 7: optical functions in the 3rd section.

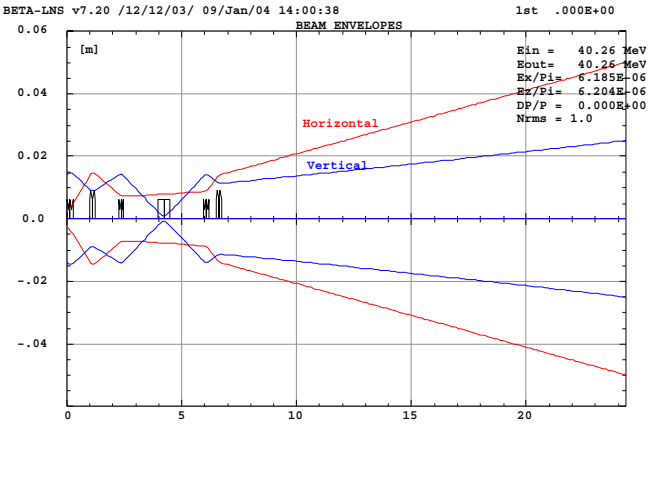

Figure 8: beam envelopes in the 3rd section.

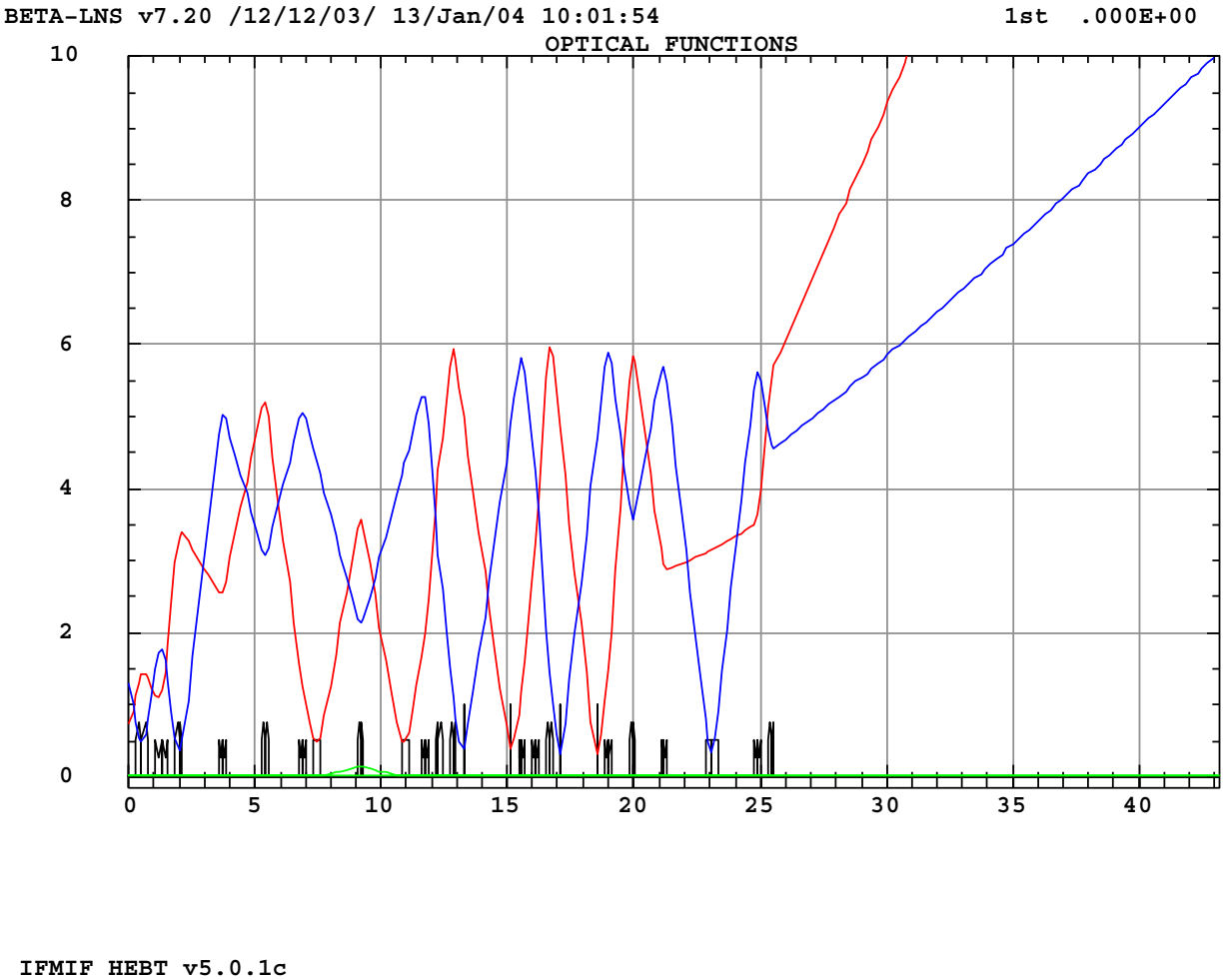

Figure 9: full line optical functions.

3 PIC SIMULATIONS

3.1 CALCULATION FRAMEWORK.

A 1,000,000 macroparticle 4D water-bag distribution is used at the input of the RFQ. The transverse rms normalised emittances used are 0.25 π.mm.mrad. The beam current is 130 mA. Multiparticle simulations are then done from the RFQ output in the full DTL. And finally, the output DTL beam distribution is injected in the HEBT line.

- Transport through the RFQs is done with TOUTATIS [6].
- Transport through the rest of the linac is done with TraceWin / PARTRAN [7] (with PICNIC [8] 3D space-charge routine, taken into account of the bunch overlap effect).

The behaviour of the beam envelope in the HEBT is plotted below.

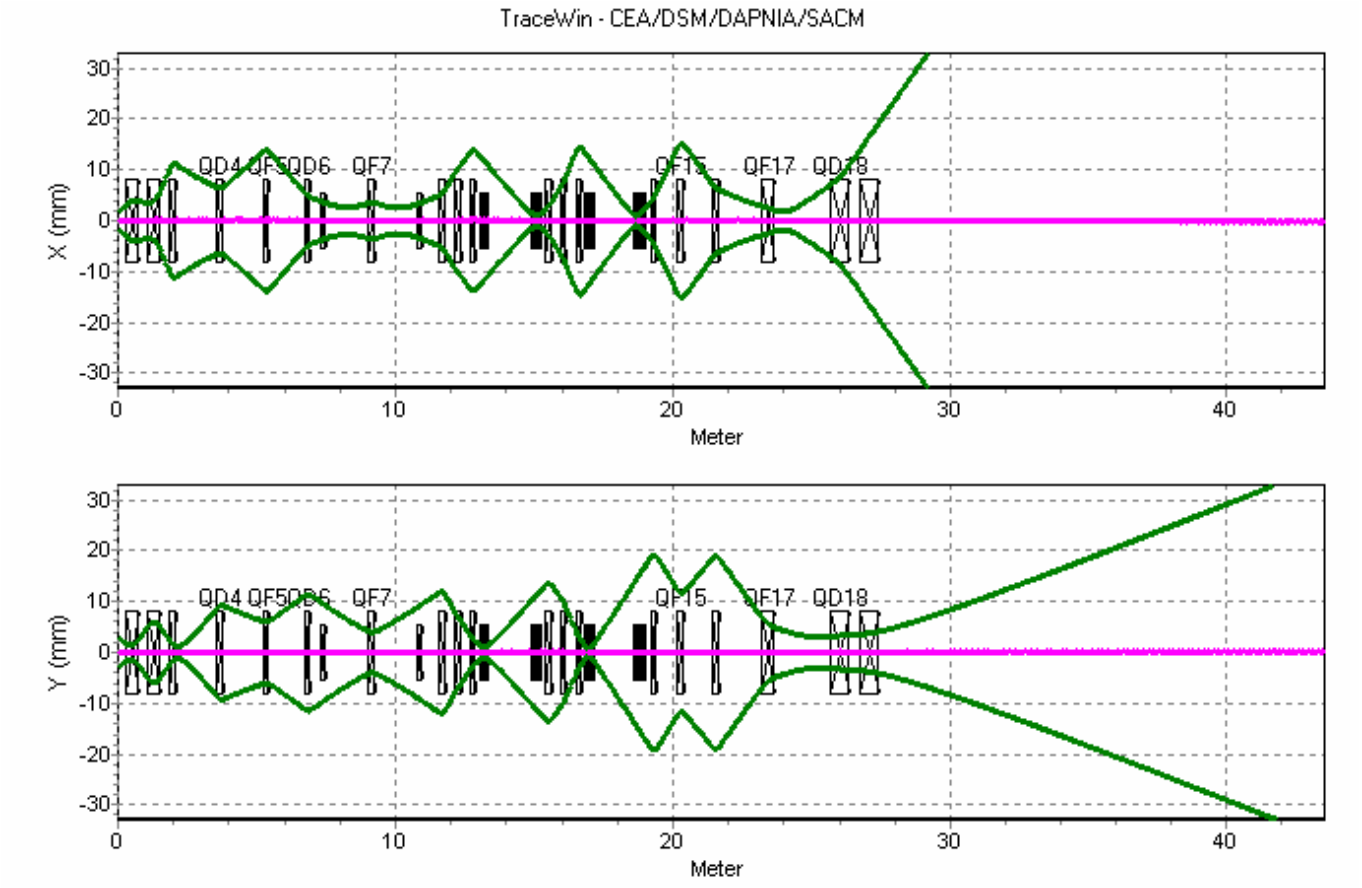

Figure 10: Transverse envelopes.

Due to the halo beam size (non-linear effect such as space-charge, non linear elements), we estimate than a beam pipe radius of 15 σ is necessary. Here, we use a beam pipe radius from 8 cm to 15 cm according to beam size. In the same time we have respected for the different magnetic elements a maximum field on the pole tip lower than 1 T. This implies an aperture lower than 5 cm for non linear lenses which is smaller than the required 15 σ. Indeed, to double the aperture in an octupole and duodecapole keeping the same strength, we have to multiply the field by 2^3 (8) and 2^5 (32) respectively. Two octupoles and two duodecapoles are used in order to reach the footprint requirement. The duodecapoles role is to improve the beam flatness by folding back the tails created

by the octupole. All the HEBT magnetic elements are listed in the following table.

Element	Length (mm)	Strength
QF1	500	6.9 T/m
QD2	500	-7.9 T/m
QF3	250	8.2 T/m
QD4	250	-5.3 T/m
QF5	250	4.5 T/m
QD6	250	-3.7 T/m
D1	3183	4.5 °
QF7	250	6.2 T/m
D2	3183	4.5 °
QD8	250	-6.1 T/m
QF9	250	1.1 T/m
QF10	250	5.2 T/m
DUO1	*400*	*0.25 T/m^5*
DUO2	*400*	*0.25 T/m^5*
QD11	250	-5.3 T/m
QD12	250	-2.9 T/m
QF13	250	7.8 T/m
OCT1	*400*	*-0.57 T/m^3*
OCT2	*400*	*0.98 T/m^3*
QD14	250	-4.6 T/m
QF15	250	6.6 T/m
QD16	250	-3.9 T/m
QF17	500	2.3 T/m
QD18	750	-0.74 T/m
QF19	750	0.04 T/m

Table 1: HEBT list of elements

3.2 OUPTUT DISTRIBUTION

The output profile is illustrated by Figure 11 and Figure 12. These results indicate that the deviations from uniformity in the flat-top region are in the range of ± 7 %, rather than the desired ± 5 % in vertical plane (see Figure 13, Figure 14, Figure 15 and Figure 16). While the horizontal beam distribution fill up better than the requirements. The peaks along the horizontal edge rise are much better than the desired 15 %. But the 0.5 μA/cm^2 beam density limit beyond 22 cm is clearly out of reach, especially in a space-charge regime.

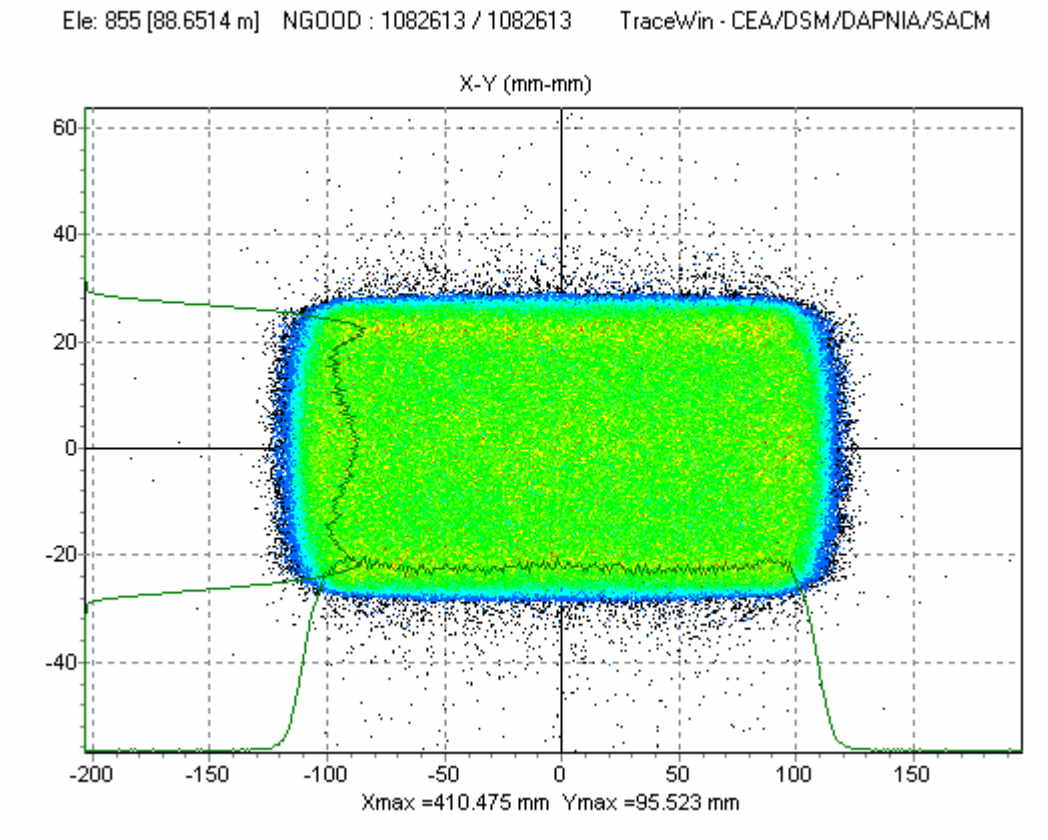

Figure 11: Output HEBT beam distribution.

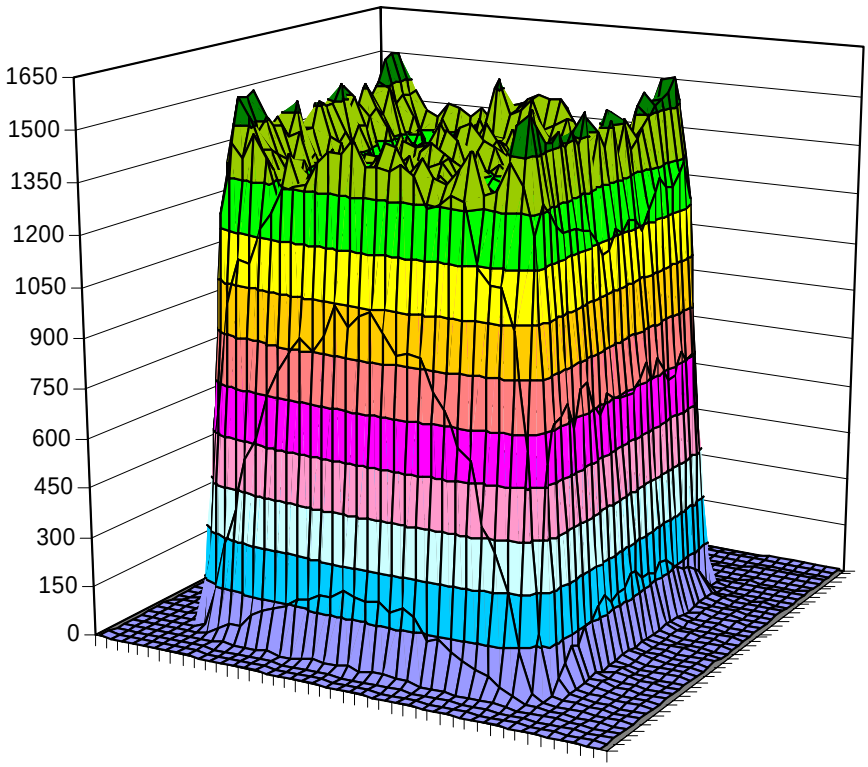

Figure 12: 3D beam distribution at the target

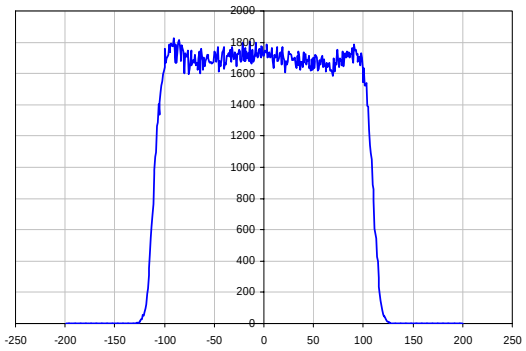

Figure 13: Horizontal beam profile.

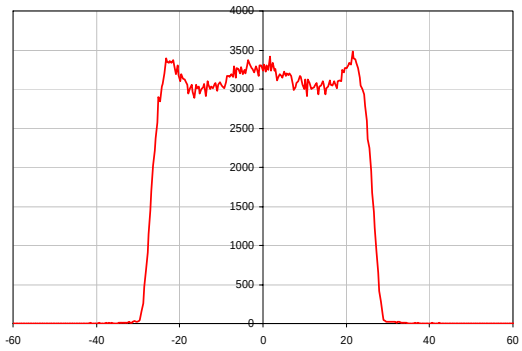

Figure 15: Vertical beam profile.

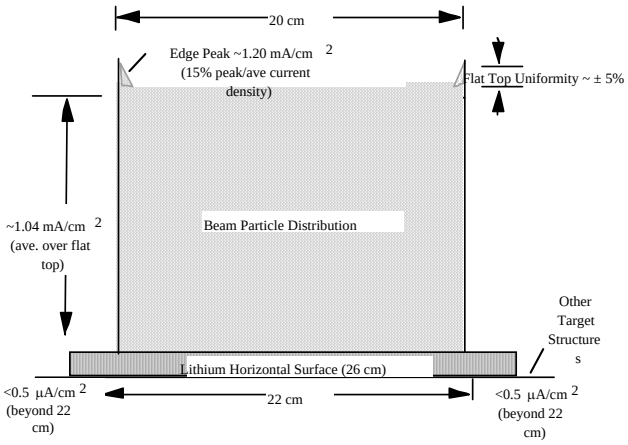

Figure 14: Horizontal requirements.

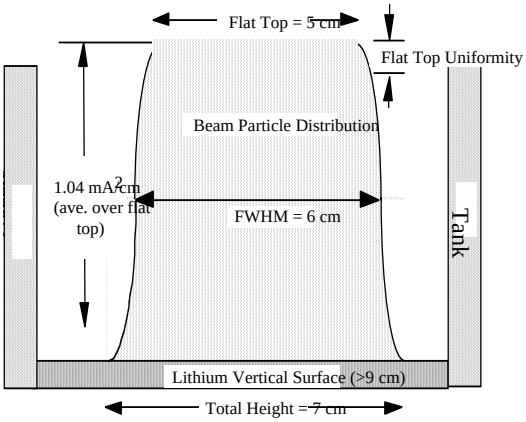

Figure 16: Vertical requirements.

3.3 BEAM LOSSES

The simulation using the beam distribution from the DTL shows losses mainly located in the non-linear lenses, where the pipe radius is the smallest (5 cm). About 44 macroparticles over 1,000,000 are lost. They correspond to about 6 μA and 240 W. The same simulation performed with an initial 4σ gaussian distribution shows no loss. For the same rms emittance, the total emittance from the DTL beam is 4 times bigger than the usual 4σ gaussian distribution (see Figure 17 and Figure 18) and 3 times bigger for the beam size. The Figure 19 shows the losses distribution in the HEBT.

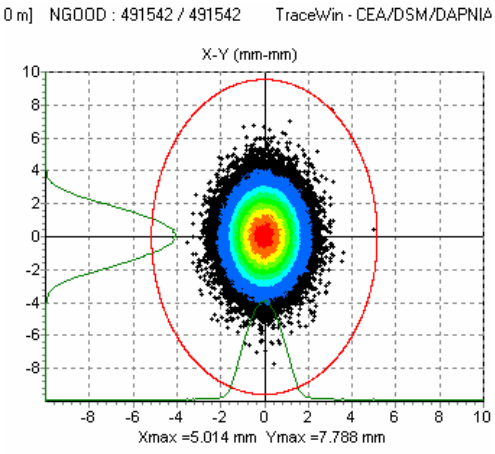

Figure 17: DTL output distribution.

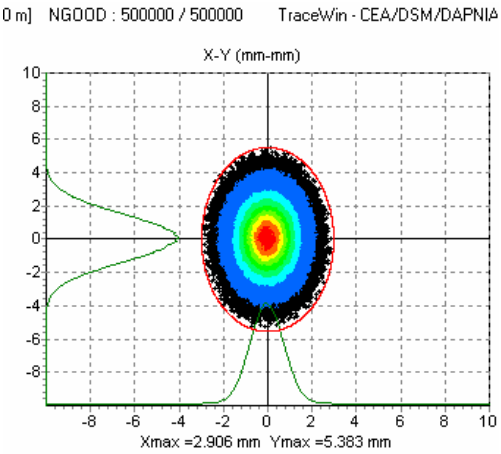

Figure 18: 4σ Gaussian.

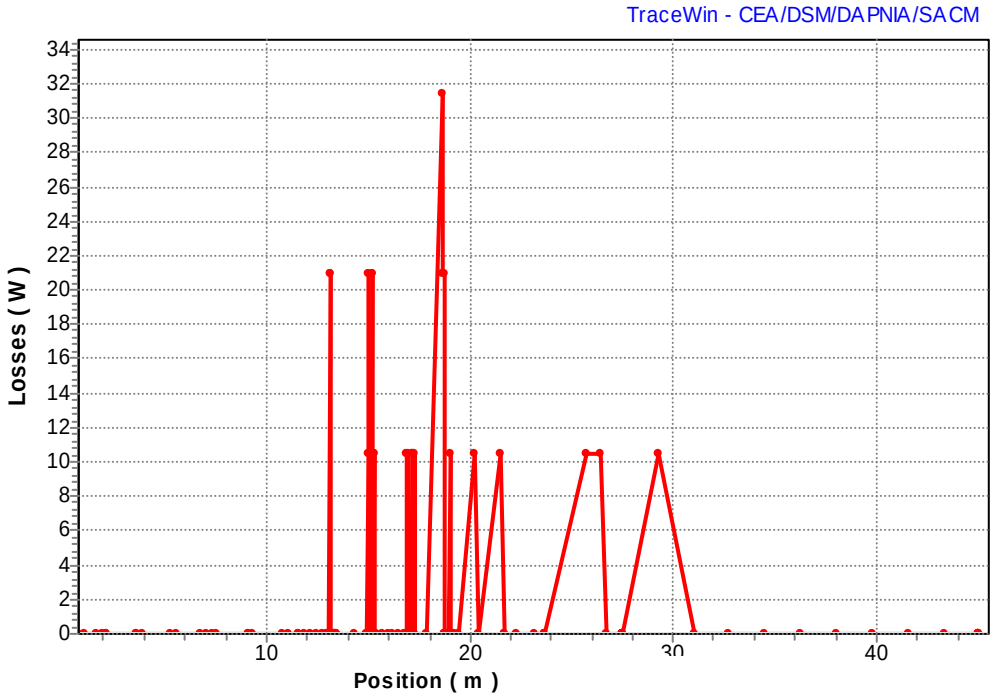

Figure 19: losses (W) along the HEBT.

A possible way to avoid losses all along the HEBT and minimize activation of the accelerator components is to reduce the beam halo with a scraper. A dedicated scraper can be designed to support more easily the losses and allow easier shielding than multipole elements. The simulation shows no loss if it is located after the achromat line. The removed beam portion corresponds to 0.02 % (1 to 2 kW). The following graph (Figure 20) represents the different beam size radii and the aperture along the HEBT. The red line corresponds to 90 % of the beam, the blue one 99%, the green 99.9% …, the black line includes the entire beam and the last black line represents the aperture. The scraper avoids the losses in the multipole lenses.

In this study, the 17 m drift between the last quadrupole and the target has an increasing aperture. This aperture should be lowered for practical reasons. As an example, if the maximum aperture is set to 200 mm (pink box), the lost beam fraction can easily be estimated by using these curves (Figure 20). Here, less than 1 particle over 10^6 will be lost.

Taking into account this point and the beam size, it appears that losses will mainly occur 23 m from the DTL end. In order to avoid these losses a solution would consist of inserting, just before the last doublet, a wall to separate the HEBT in 2 parts according to the radioprotection level.

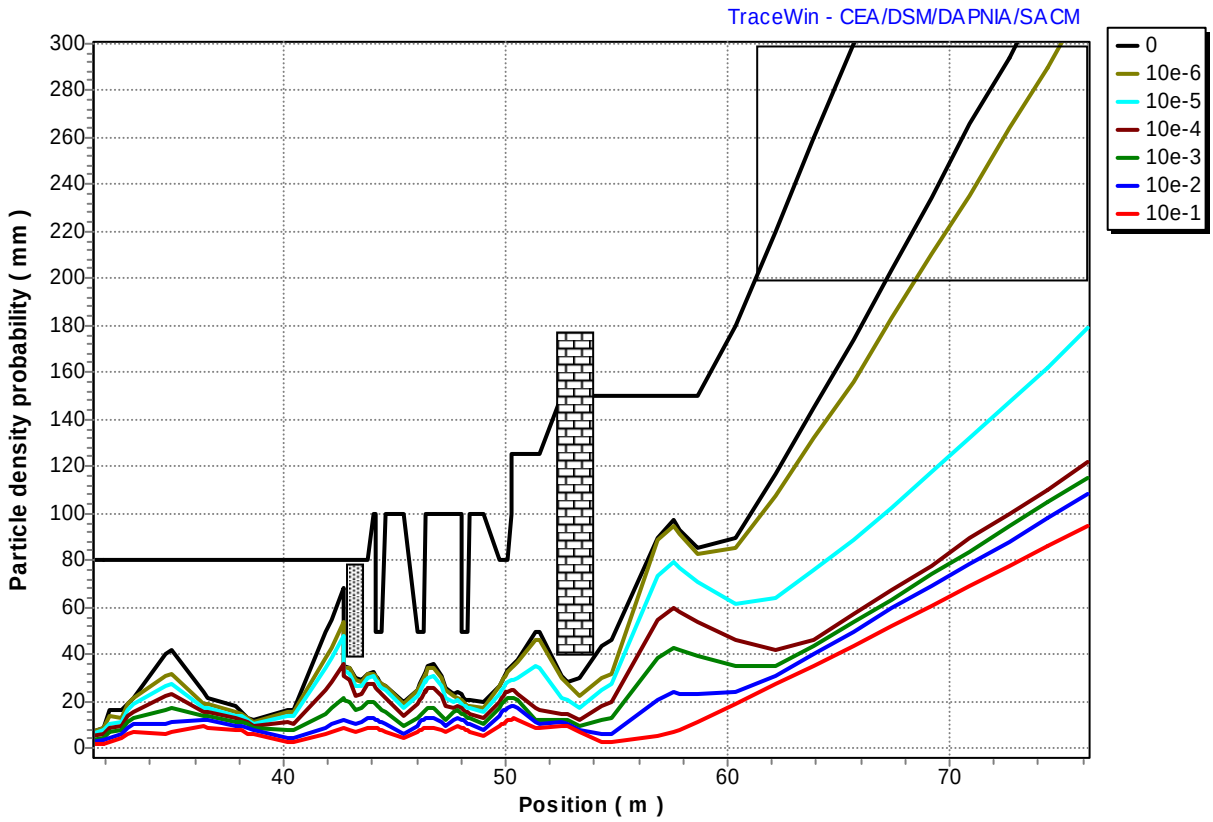

Figure 20: Beam size radii along the HEBT.
(10^{-1} corresponds to 90% of the beam, 10^{-2}→99%, 10^{-3}→99.9% ...and the last black one: 100%

4 SENSITIVITY TO LINAC ELEMENT ERRORS

4.1 INTRODUCTION

In real life, the linac elements are a little bit different than expected. Quadrupoles may have a wrong position, be tilted, or have a wrong gradient. Cavities may have a wrong position, be tilted, or have a wrong field (phase and/or amplitude). An imperfect beam position measurement has also to be taken into account.

Two families of errors may occur:

- Static errors: the effect of these errors can be detected and cured with appropriate diagnostic and correctors. For example, beam position measurement coupled with steerers can compensate the quadrupole or cavities misalignments. The correction strategy should be known to be able to estimate the impact of static errors on beam dynamics.
- Dynamic errors: the effect of these errors is assumed to be uncorrected. Fortunately, they have usually lower amplitude than static errors. There are, for example, the vibrations or the RF field variations (in phase or amplitude). They are responsible of orbit oscillations around the corrected orbit (this notion of orbit is also extended in the longitudinal motion).

The effect of the static errors depends on the orbit control system. A correction scheme has been

studied. The locations of the beam position monitors and the associated steerers are described in the paragraphs describing the structures. The effect of this correction scheme is described in this paragraph.
Errors with different amplitudes have been used depending on the linac section. The amplitudes of the errors are summarized bellow. For an error amplitude *A*, the element error has uniform probability to be between –*A* and +*A*.

	Static	**Dynamic**
RFQ		
Machining transverse defect (mm)	±0.05	
Machining longitudinal defect (Z) (mm)	±0.05	
perpendicular tilt by segment (mm)	±0.1	
parallel tilt by segment (mm)	±0.1	
perpendicular displacement by segment (mm)	±0.1	
Parallel displacement by segment (mm)	±0.1	
MATCHING LINE RFQ-DTL		
Quadrupole gradient (%)	±0.5	±0.05
Quadrupole displacement (mm)	±0.1	±0.005
Quadrupole rotations (X,Y) (deg)	±0.15	±0.015
Quadrupole rotations (Z) (deg)	±0.25	±0.025
BMP accuracy (mm)	±0.1	
Cavity displacement (mm)	±0.1	±0.01
Cavity rotations (X,Y) (deg)	±0.05	±0.005
Cavity field phase (deg.)	±0.1	±0.01
Cavity field amplitude (%)	±0.1	±0.01
DTL		
Quadrupole gradient (%)	±0.5	±0.05
Quadrupole displacement (mm)	±0.1	±0.01
Quadrupole rotation (X,Y) (deg)	±0.15	±0.015
Quadrupole rotation (Z) (deg)	±0.25	±0.025
BMP accuracy (mm)	±0.1	
Cavity field phase (deg.)		±0.01
Cavity field amplitude (%)		±0.01
Tank displacement (mm)	±0.1	±0.01
Tank rotations (X,Y) (deg)	±0.002	±0.0002
Tank field phase (deg.)	±1	±0.01
Tank field amplitude (%)	±1	±0.01
HEBT LINE		
Quadrupole gradient (%)	±0.5	±0.05
Quadrupole displacement (mm)	±0.1	±0.002
Quadrupole rotation (L=25 cm) (X,Y) (deg)	±0.03	±0.003
Quadrupole rotation (Z) (deg)	±0.25	±0.025
Multipole lens gradient (%)	±0.5	±0.05
Multipole lens displacement (mm)	±0.1	±0.02
Multipole lens rotation (X,Y) (deg)	±0.02	±0.002
Multipole lens rotation (Z) (deg)	±0.25	±0.025
BMP accuracy (mm)	±0.1	

The rotation angles (X,Y) have been calculated assuming an independent motion of element edges with amplitude defined in dx and dy. It corresponds to about $\arctan\left(\sqrt{2}\cdot\frac{dx}{Le}\right)$ with *Le* the element length.
There is no error on the dipole elements in the present study.

4.2 CORRECTION SCHEME

A correction-set is constituted of two steerers which kick the beam in both planes. They are associated with two Beam Position Monitors which measure the beam centroid in both planes. To correct beam misalignments in the DTL, such couple of steerers are placed into the last tubes of each tank and a couple of BPM are placed between tanks. In the HEBT, 6 correction-sets are necessary to control efficiently the beam central trajectory. The correction scheme is efficient in the DTL (residual orbit radius is lower than 1 mm) and is more difficult in the HEBT line, especially in the last 17 m drift which is very sensitive.
At the present time, we did not include in our simulation specific diagnostic to correct the gradient errors which cause mainly mismatching. Thus, we consider that the error studies results below show a worse beam behavior that the normal operating mode where some specific diagnostics are used to match the beam to take into account the machine errors.

The rms value of the residual orbit along the DTL and HEBT is plotted on Figure 21. It is the result of a statistics over 100 linacs. We notice that the rms jitter centroid position at the target is about 6 mm. It is due to the dynamic errors (vibrations: 5 μm for DTL, 2 μm for HEBT). In order to reduce the jitter, vibration tolerances have to be significantly reduced. We should notice that they are already challenging.

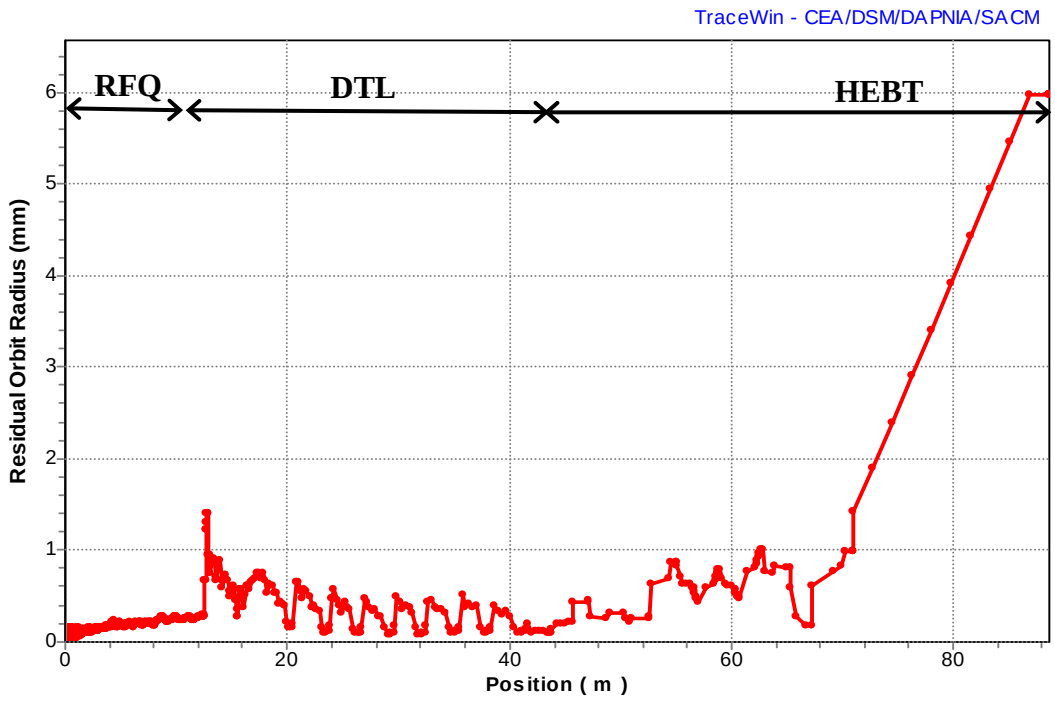

Figure 21: Residual orbit RMS value along the linac.

4.3 ERROR STUDIES

4.3.1 HEBT line

We study first the HEBT line alone. The transport of a 100,000 macroparticle beam has been simulated in a set of 110 different HEBT lines with all combined errors on each element. The beam distribution from DTL has been used. Figure 20 shows the statistical distribution of the particles along the HEBT. The red line corresponds to 90 % of the beam; the blue one 99%..., the black line includes the entire beam and the last black line represents the aperture. We observe that 1200 W are dissipated in the scraper. For a pipe radius limited to 200 mm in the last drift, 1 particle over 10^6 will be lost.

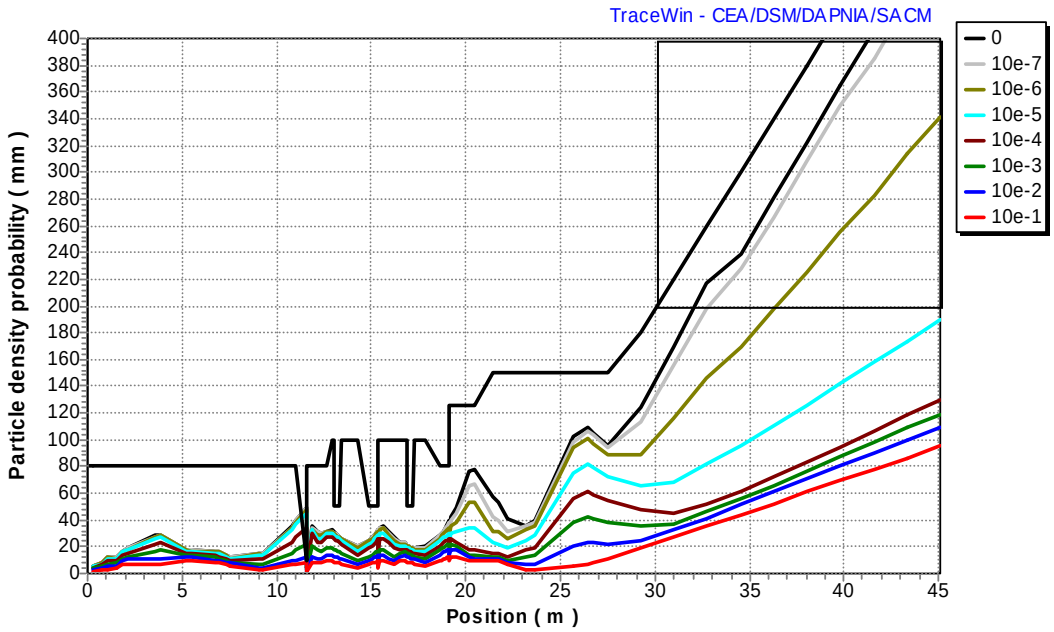

Figure 22: Beam size radii along the HEBT.
(10^{-1} corresponds to 90% of the beam, 10^{-2}→99%, 10^{-3}→99.9% ...and le last black one: 100%

The distribution in Figure 23 obtained from the superposition of 110 different simulated linacs with all the combined errors. It represents the probability to reach this density at the target. We notice that the distribution is still close to the requirements. The imperfections mainly degrade the beam fringes and increase the beam noise.

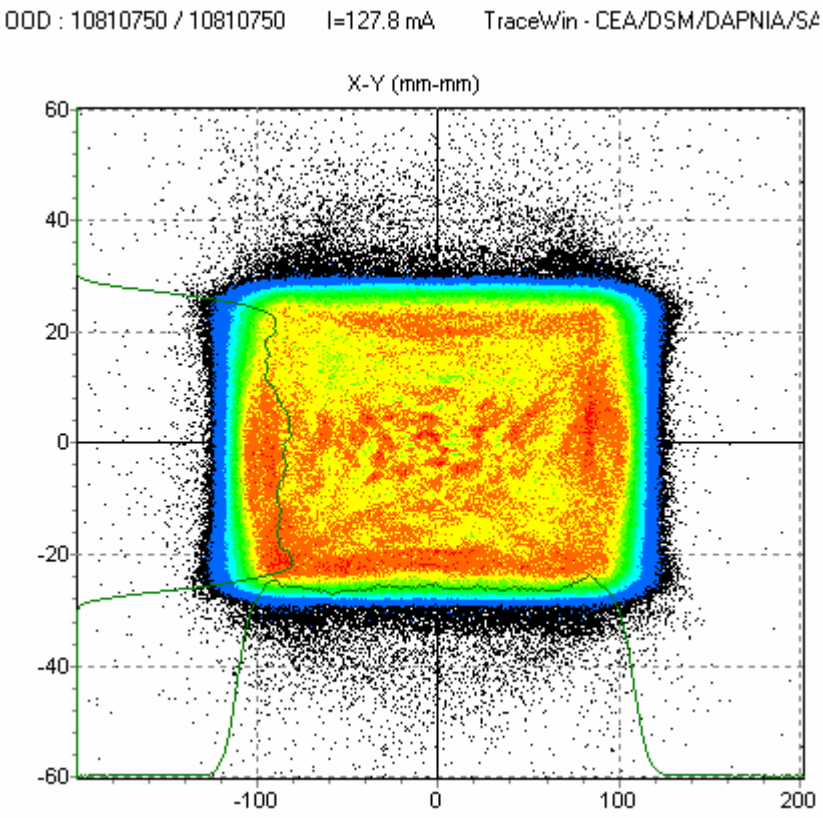

Figure 23: Output HEBT beam distribution (HEBT error).

4.3.2 End-to-End errors study

The linac (RFQ-DTL) used in this study is the IFMIF reference design [9]. The transport of a 100,000 macroparticles beam has been simulated in a set of 110 different linacs with all combined errors on each element. The simulation begins at the RFQ input. All the previously listed errors are used. Figure 24 shows the envelope behavior along the IFMIF design without error. Figure 25 and Figure 26 represent the different beam size radii along the RFQ, DTL and HEBT. Figure 27 shows the beam distribution at the target taking into account all the errors. It has to be repeated that all these results include un-corrected mismatch errors. The output distribution characteristics are close to the requirement except the 0.5 $\mu A/cm^2$ beam density limit beyond 22 cm.

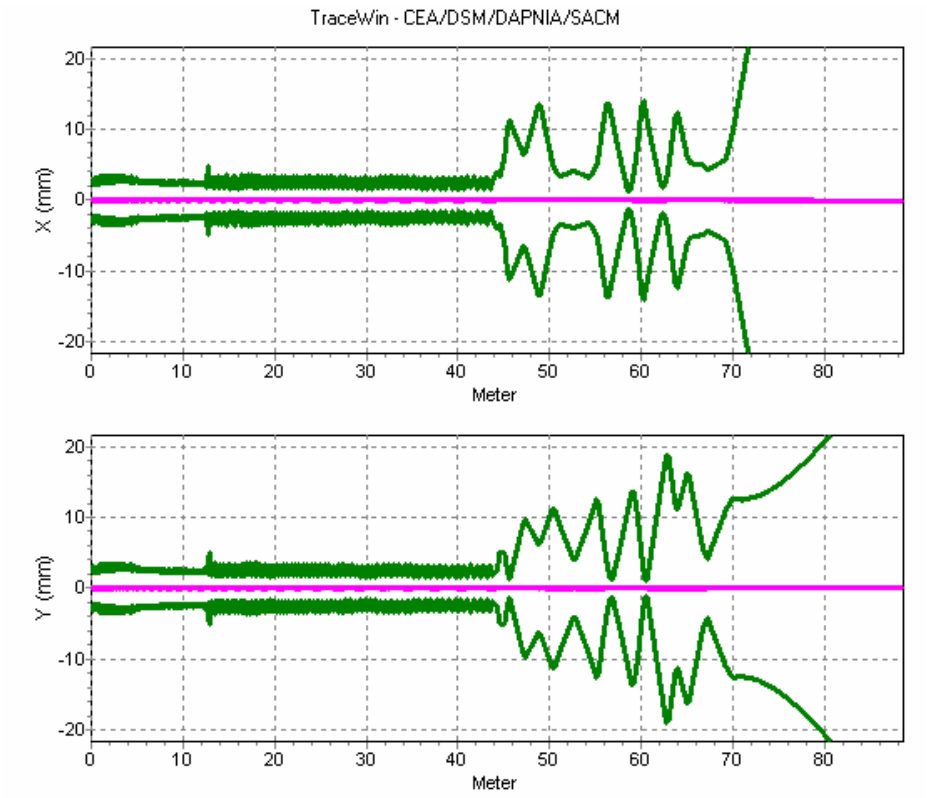

Figure 24: Transverse envelopes (RFQ-DTL-HEBT).

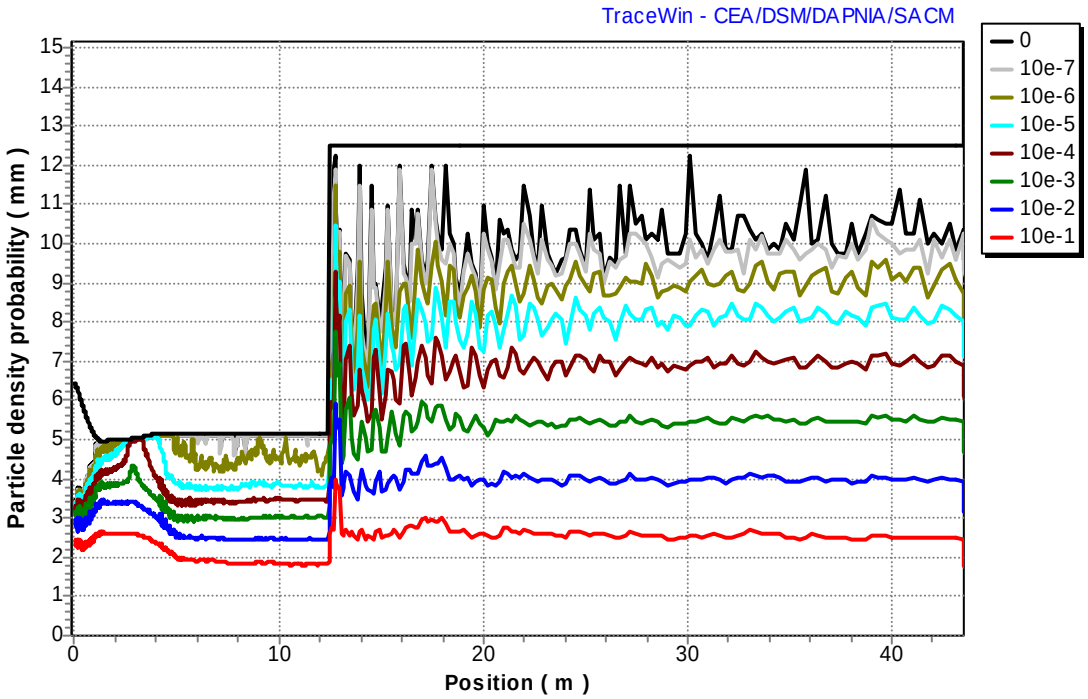

Figure 25: Beam size radii along the RFQ and DTL.
(10^{-1} corresponds to 90% of the beam, 10^{-2}→99%, 10^{-3}→99.9% ...and the last black one:100%

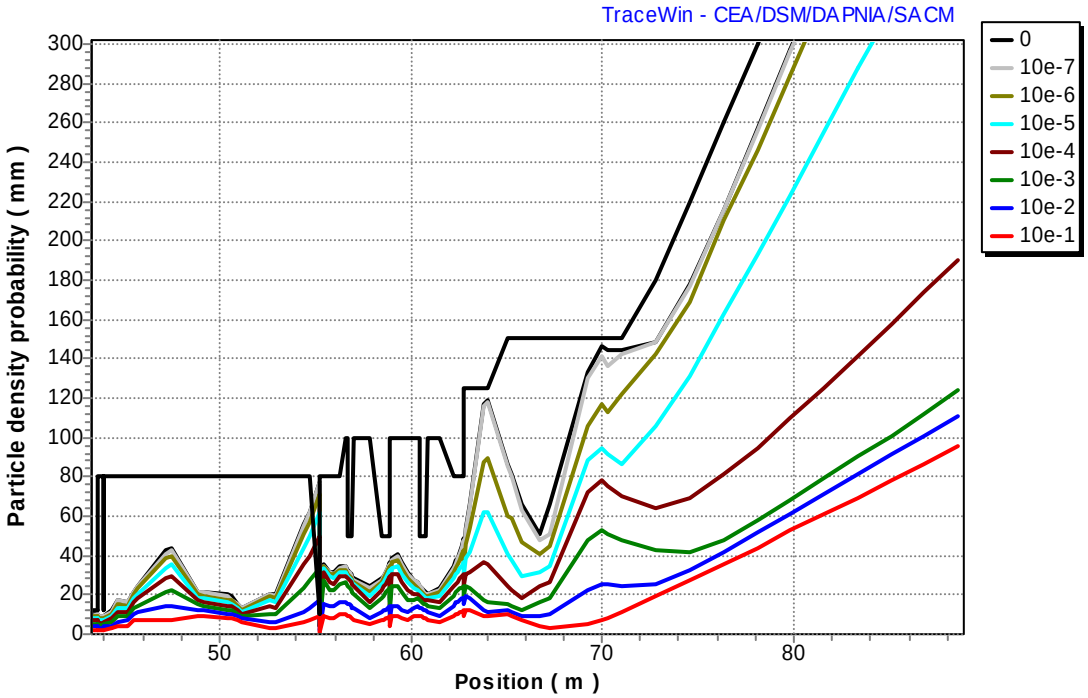

Figure 26: Beam size radii along the HEBT.
(10^{-1} corresponds to 90% of the beam, 10^{-2}→99%, 10^{-3}→99.9% ...and the last black one:100%

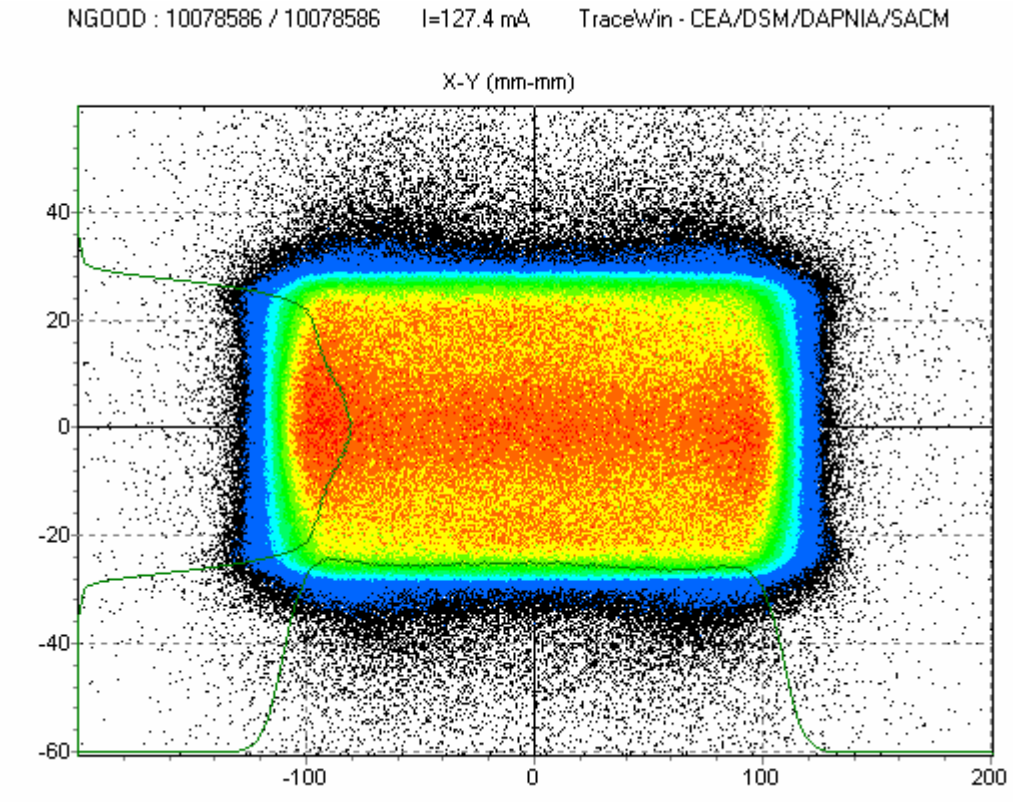

Figure 27: Output HEBT beam distribution (Full linac error)

Figure 28 gives the loss repartition along the structure and the corresponding dissipated power. This repartition is 1.98 % in the RFQ, 0.18 % in the DTL and 0.17 % in the HEBT. Remember that no matching has been used to control the beam mismatch due to focalization errors, while it will be partially corrected in real operation.

The first end-to-end errors study made in 2002 did not show any loss in the DTL [9]. Two reasons explain the results of this paper:

- More errors have been taken into account like vibrations, phase and field errors, tank displacements and vibrations, BPM errors…
- The statistics was 100 runs of 10,000 macro particles compared to the 100 runs of 100,000 macro particles of the present study. It didn't allow to observe loss intensity smaller than 128 nA.

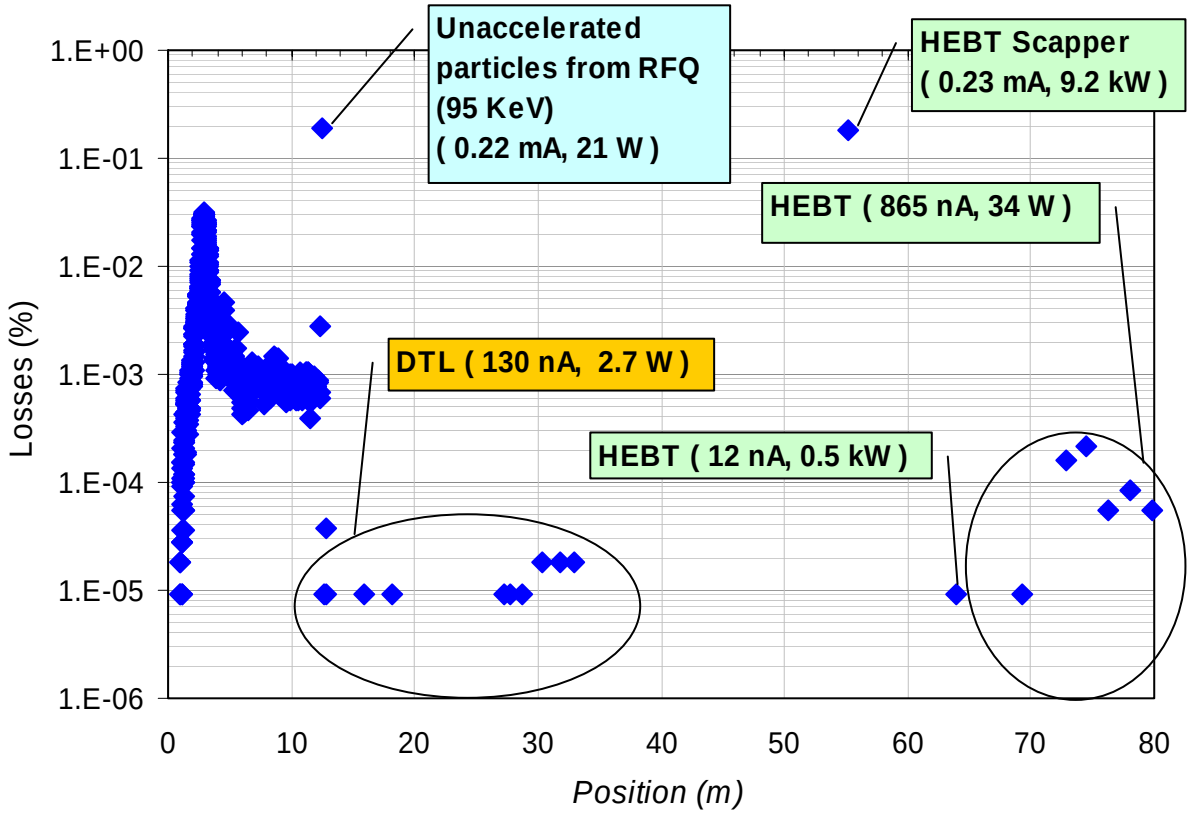

Figure 28: Losses repartition along the structure.

Several methods can be explored in order to reduce these losses:

- change the DTL design without increasing the number of diacrode, in order to increase the aperture drift tube from 12.5 mm to 14 mm or more (see following section),

- the RFQ machining tolerance could be slightly decreased.

Concerning the HEBT losses, the extra dissipated power in the scraper compared to the nominal case (1 kW) comes from the beam mismatch. In normal operating mode the beam will have to be matched in order to control this power. Moreover, this scraper could be an interesting diagnostics to manage that.

4.4 ALTERNATE DTL DESIGN

The main losses in the DTL are located after the 4th tank. They can be easily avoided by using 2 different quadrupole lengths rather than only one along the DTL (present design). Using a longer quadrupole for the longer drift tubes allows to increase the inner drift tube radius without increasing the outer radius and the RF power.

Another method is simply to scale all the drift tube and quadrupole dimensions like described below. The aperture may then be increased without an enhancement of the maximum field on the pole field tip.

Drift tube aperture	**: 1.25 cm**	**→ 1.4 cm**
Drift tube radius	: 9.6 cm	→ 9.75 cm
Quadrupole length	: 7.8 cm	→ 8.6 cm
Quadrupole radius	: 7.6 cm	→ 7.75 cm

Thus, no extra power will be required for the quadrupole power supply. The copper drift tube surface is slightly increased, but, in the reference design, only one third of the available power is used in the last tank. So, a new DTL design has been generated with the GENDTL code [10] and the results show it is possible to increase the aperture with o no density increase of the power.

	Reference	**1.4 cm**
Number of diacrode	10	10
Number of cells	119	121
Total power (Pt)	6.34 MW	6.46 MW
Power dissipation	1.86 MW	1.98 MW
Beam power (Pb)	4.48 MW	4.48 MW
Efficiency (Pb / Pt)	71 %	69 %

Table 2: Reference and new DTL characteristics

Figure 29 shows the beam radial distribution in the DTL. An extrapolation can give an idea of the losses for larger DTL aperture.

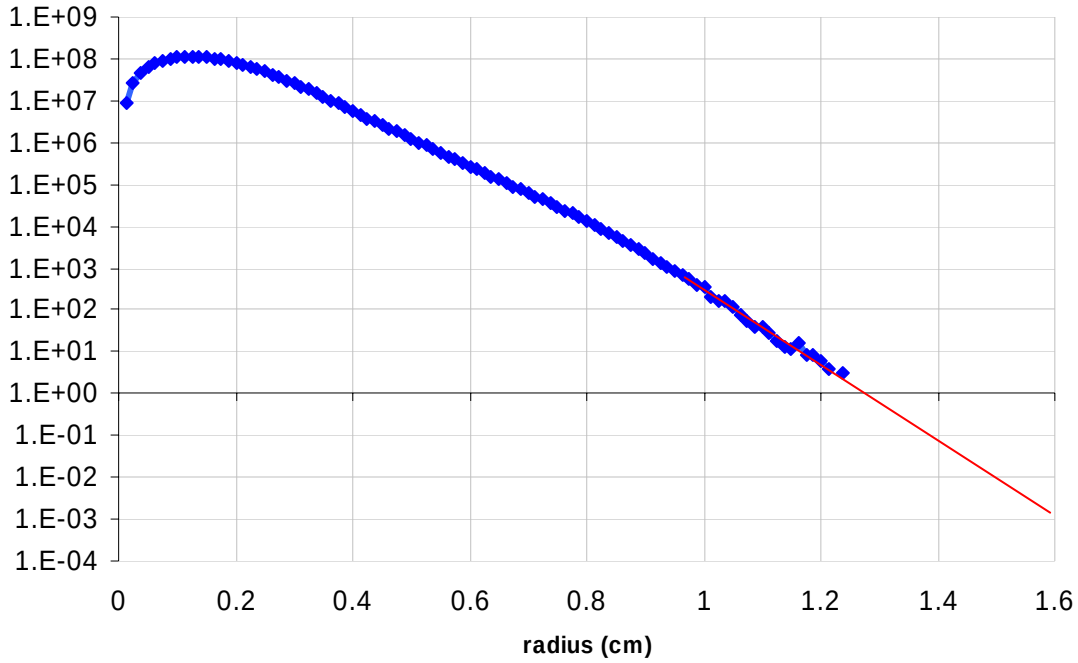

Figure 29: Particles repartition along the DTL (red line is the extrapolated curve).

5 CONCLUSION

We demonstrated the existence of a High Energy Beam Transfer design solution.
The end-to-end studies show manageable losses if we accept scrapers (localised losses, easier shielding and protection of multipole elements). The reduction of losses in the HEBT line can be achieved. Increasing the multipole lens aperture allows to reduce the beam part dissipated on the scraper and may allow to remove it. A specific study would be needed on this issue.
We managed some room for insertion of radioprotection walls against the losses at the end of the last 17 meters long drift tube.
This last drift implies very strict dynamic tolerances on the previous elements. In this design, their values are challenging but exist in other machine like the photon machines.
Work is still needed to improve the design, for instance, optimizing the DTL aperture.
All the beam characteristics requirements at the target can be reached using multipole lenses, excepted for the horizontal edges (0.5 $\mu A/cm^2$ beam density limit beyond 22 cm).

References

[1] : Ref DSM/DAPNIA 03-72: CEA-DSM-DAPNIA-SACM contribution to the IFMIF KEP phase June 2000 to December 2002

[2]: JAERI-Tech 2003-005, IFMIF-KEP, Key element technology phase report.

[3]: J. Payet. BETA code

[4]: F. Meot, T. Aniel, Principles of the non-linear tuning of beam expander NIM A379 (1996)

[5]: F. Meot, T. Aniel, On beam uniformization by non-linear optics CEA/DSM/GECA/ 95-05, July 1995

[6]: R. Duperrier, "Dynamique de faisceaux intenses dans les RFQs", Université Paris sud Orsay, n° 6194, juillet 2000.

[7]: R. Duperrier, N. Pichoff, D. Uriot, "CEA Saclay codes review", ICCS conference, Amsterdam, 2002.

[8]: N. Pichoff, J. M. Lagniel, and S. Nath, "Simulation Results with an Alternate 3D Space Charge Routine, PICNIC," Proceedings of the XIX International Linac Conference, p 141, Chicago.

[9]: R. Duperrier, D. Uriot , N. Pichoff , R. Ferdinand "Beam dynamics end to end simulations in IFMIF Linac" EPAC 2002, Paris.

[10]: D. Uriot, N. Pichoff, "GENDTL", internal report CEA/DSM/DAPNIA/SEA/2000/46